Synthesis of Nanoporous Network Materials with High Surface Areas from the Cooperative Assemblage of Alkyl-Chain-Capped Metal/Metal Oxide Nanoparticles

Driss Mrabet, M. Hassan Zahedi-Niaki, and Trong-On Do*

Department of Chemical Engineering, Laval University, Quebec G1K 7P4, Canada

Received: December 24, 2007; In Final Form: February 26, 2008

A simple route for the synthesis of a new class of porous metal/metal oxide nanoparticle (NP) materials such as Cu−TiO_2, Au−ZrO_2, Cu−ZrO_2, and Au−TiO_2 NPs through the cooperative assembly of presynthesis hydrophobic oleic acid (OA)-capped metal and metal oxide NPs is reported. In such a way, the synergistic interaction between metal and metal oxide NPs has gained significant interest owing to new properties that arise at the metal−metal oxide interface. Various technique including XRD, N_2 adsorption/desorption isotherms, FTIR, TEM, XPS, and catalytic test were used to monitor the physicochemical and catalytic properties of these materials. The results revealed that these porous materials exhibit homogeneous dispersion in between metal and metal oxide NPs, high surface area, and narrow interparticle pore size distribution. The catalytic properties of these metal/metal oxide NP solids (even Cu oxide NP catalysts, e.g., no noble metal catalyst) in the CO oxidation reaction are better than those of commercial noble metal catalyst (Pt/Al_2O_3) and the conventional metal oxide-supported Cu catalysts. Based on this synthesis approach, a variety of nanoporous multicomponent solids of both metal and metal oxide with desired proportions can be synthesized.

Introduction

Nanoparticles (NPs) with 1−10 nm in size have unique properties, owing to their inherent large surface-to-volume ratio and quantum size effects, which differ from those of the corresponding bulk materials. Significant progress from many research groups has been made on the synthesis of nanoparticles over the past two decades. A variety of chemical methods have been developed for generating uniform-sized nanoparticles with well-controlled sizes and from a large range of materials such as metals, metal oxides, and metal chalcogenides.[1−3] Recently, we have also reported a new approach for the synthesis of small/uniform nanozeolites with hydrophobic surface and high external surface area, which is applicable to different kinds of zeolite structures.[4] Moreover, to achieve a high catalytic activity, metal NPs are generally dispersed on oxide supports. Zheng and Stucky[5] demonstrated a general strategy for the synthesis of metal NPs highly dispersed on oxide supports using presynthesized hydrophobic metal NPs. Zeolite nanoclusters coated onto the walls of mesoporous materials were also reported by our group.[6,7] Such materials are considered of potential applications as catalysts due to their hydrophobic surface and high surface area, reduced diffusion pathways, and exposed active sites.[4−7]

The self-assembly of monodisperse NPs into a well-defined three-dimensional nanostructure has rapidly attracted a growing interest.[8−10] In particular, mesoporous metal/oxide NP solids with controlled particle sizes could provide catalytic performance over conventional catalysts. Furthermore, the interaction between metal NPs and metal oxide NPs has gained significant interest owing to new properties that arise at the metal/metal oxide interface.[11−13] This type of catalyst exhibits high catalytic activity toward different types of reactions, such as the NO_x reduction and the CO oxidation at low temperatures. Corma et al. have shown that nanocrystalline CeO_2-supported Au catalysts are 2 orders of magnitude more active than conventional Au/CeO_2 catalysts for the CO oxidation.[14] This might be due to a synergetic interaction between Au NPs and nanosupport at the interface, such that the support does not act as an inert carrier but intervenes in the catalytic reactions.[14] Only a few examples of this type of porous metal/metal oxide particles are yet known.[14−18] The synthesis of these materials still remains particularly challenging.

In order to explore new properties arising at the interface between metal nanoparticle and metal oxide nanoparticles, herein we report a simple route for the synthesis of a new class of metal/metal oxide NPs solids with high surface area and interparticle porosity through the cooperative assembly of presynthesized hydrophobic NPs of both metal and metal oxide. To illustrate our approach, Au and Cu as metal nanoparticles, and TiO_2 and ZrO_2 as metal oxide nanoparticles were selected in this study. Toluene and oleic acid (OA) were used as solvent medium and capping agent, respectively. The catalytic activity in the CO oxidation reaction was also reported.

Experimental Section

Material Preparation. In this study, the synthesis of nanoporous metal/metal oxide nanoparticles (NPs) materials through the cooperative assembly of oleic acid (OA)-capped NPs consists of two steps: (1) Synthesis of monodisperse OA-capped metal nanoparticles (e.g., Cu, Au) and OA-capped metal oxide nanoparticles (TiO_2, ZrO_2) in toluene media. The resulting hydrophobic NPs of both metal and metal oxide were separately dispersed in toluene. (2) The metal NPs solution and the metal oxide NPs solution with desired proportions were mixed, and clear/transparent solutions were obtained. These mixtures were followed by evaporation. The dispersion of metal and metal oxide NPs is then locked in place by calcination.

1. Synthesis of OA-capped metal nanoparticles and OA−metal oxide nanoparticles. (i) Synthesis of metal nanoparticles:

* Corresponding author. E-mail: Trong-On.Do@gch.ulaval.ca.

10.1021/jp7120593 CCC: $40.75
Published on Web 04/15/2008

TABLE 1: Physicochemical Properties of Different Types of Nanoporous Materials: Metal Nanoparticles (NPs), Metal Oxide NPs, and Metal/metal Oxide NPs Materials

no.	sample	metal (wt %)	S_{BET} (m^2/g)	pore radius (nm)	pore volume (cm^3/g)	particle diameter[b] (nm)	S_{Th}[a] (m^2/g)	particle diameter[c] (nm)
calcined sample								
1	ZrO_2 NPs		108	1.85	0.085		145	7.5 ± 0.7
2	TiO_2 NPs		165	4.78	0.51		170	8.0 ± 0.8
3	Au/ZrO_2 NPs	0.25	116	1.86	0.09		145	7.6 ± 0.7
4	Cu/ZrO_2 NPs	3.4	130	1.72	0.11		145	7.8 ± 0.7
after catalytic test		132	1.75	0.10				
5	Au/TiO_2 NPs	0.23	160	2.57	0.30		170	8.4 ± 0.8
6	Au/TiO_2 NPs	1.32	170	3.40	0.33			8.4 ± 0.8
7	Cu/TiO_2 NPs	3.8	162	1.82	0.15		169	8.2 ± 0.8
after catalytic test			164	1.85	0.16			
as-made sample								
1	Au NPs					3.1 ± 0.4		
2	Cu NPs					5.0 ± 0.6		
1	ZrO_2 NPs					7.0 ± 0.7		7.2 ± 0.7
2	TiO_2 NPs					8.5 ± 0.8		8.0 ± 0.8

[a] Surface area calculated from TEM average particle size (assuming spherical particle): $S_{th} = 6000/(\rho d)$, where ρ and d are the material density ($\rho_{Au} = 19.3$ g/cm^3, $\rho_{Cu} = 8.92$ g/cm^3, $\rho_{anatase} = 3.9$ g/cm^3, and $\rho_{Zircone} = 5.89$ g/cm^3) and particle diameter (nm), respectively. [b] Particle size is estimated from TEM images. [c] Particle size (d) determined from XRD patterns using the Scherrer equation for metal oxide NPs. The (101) plane corresponding to the 2θ peak at 25.30° for the anatase phase of titania, and the (111) plane corresponding to 30.32° for the cubic phase of zirconia used for the crystal size determination.

in a typical procedure, for copper nanoparticles, copper(II) acetate ($Cu(OAc)_2$, H_2O; 400 mg) was dissolved in a mixture of oleic acid (OA; 2 g), oleylamine (OLA; 1.33 mg), and toluene (200 mL). A solution of tetrabutylammonium borohydride (TBAB; 3 mg) in toluene (200 mL) was then added to the above copper solution, yielding a colorless complex. After being stirred for 1 h at ambient temperature, the complex was decomposed by adding 20 mL of anhydrous ethanol; the solution color changed to deep red, indicating the formation of metallic copper nanoparticles. The latter was precipitated by adding excess of ethanol. The deep red precipitate was collected by centrifugation and was then immediately dispersed in 50 mL of toluene, yielding a completely transparent solution. Gold nanoparticles were synthesized according to Brust et al.'s method (ref 19). (ii) Metal oxide nanoparticles such as TiO_2 and ZrO_2 were synthesized with a two-phase procedure according to the method of ref 20. The nanoparticles were precipitated from the organic phase by adding an excess of ethanol and further isolated by centrifugation. The nanoparticles were then dispersed in toluene, and this operation was repeated several times.

2. Nanoporous metal/metal oxide materials (e.g., Cu/TiO_2, Cu/ZrO_2, Au/TiO_2, and Au/ZrO_2 NPs) were prepared by mixing desired proportions of metal and metal oxide nanoparticles containing toluene solutions (see Table 1). The resulting homogeneous dispersion was followed by evaporation in a rotavapor and then to dry at 80 °C for 24 h. The as-prepared samples were then heated at a constant rate of 5 °C min^{-1} in flowing N_2 to 300 °C, followed by heating in flowing air to 550 °C and kept at this temperature for 2 h. The elemental analysis was performed by ICPAES (induced coupled plasma atomic emission spectroscopy).

Characterization and CO Oxidation Reaction. Transmission electronic microscopy (TEM) images were obtained using a JEOL JEM 1230 transmission electron microscope operating at 120 kV. The dispersed nanoparticles samples were prepared by dipping 200 mesh carbon-coated copper grids into the dilute solution of isolated nanoparticles in toluene and immediately evaporated at ambient temperature. The metal/metal oxide NPs solid catalysts samples were however finely dispersed in ethanol, and then a drop of a powder suspension was deposited onto the copper carbon grid. The surface composition of the prepared materials at different steps of treatment was analyzed using a photoelectron spectrometer (VG, ESCA-3).

X-ray diffraction (XRD) measurements were carried out on a Siemens D5000 X-ray diffractometer using filtered Cu Kα ($\lambda = 1.540\,62$ Å) radiation (40 kV, 30 mA), 0.02° step width, and an acquisition time of 1.2 s per step. The average crystallite size was calculated using from the broadening of the XRD peaks using the Scherrer formula: $d = 0.9\lambda/(w - w_1)\cos(\theta)$, where d is the crystal diameter, w and w_1 are the half-intensity width of the relevant diffraction peak and the instrumental broadening, respectively, λ is the X-ray wavelength, and θ is the angle of diffraction. Because almost cubic phase for ZrO_2 nanoparticles and only the anatase phase for TiO_2 NPs were observed, the following reflections—the (101) plane corresponding to the 2θ peak at 25.30° for the anatase phase of titania and the (111) plane corresponding to 30.32° for the cubic phase of zirconia—were used for the crystal size determination.

Nitrogen adsorption/desorption isotherms were performed by using the Quantachrome Autosorb-1 system. Prior to measurements, all samples were degassed at a temperature of 200 °C for at least 5 h. The specific area was calculated from the linear part of BET equation ($P/P_0 = 0.05-0.3$). The pore-size distribution was obtained from the analysis of the desorption branch of the isotherms using the BJH (Barret–Joyner–Halenda) model.

Catalytic test (CO oxidation): all catalytic tests were carried out with a high hourly space velocity (GHSV, e.g., short contact time) due to the fact that the subambient temperature experimental setup was not available in our laboratory. It should, however, consider that with a shorter contact time the CO conversion curve as a function of reaction temperature can be shifted to higher temperatures. A flow fix-bed microreactor was used to investigate the catalytic activity of Au/oxide NPs and Cu/oxide NPs catalysts. By comparison, a commercial Pt/Al_2O_3 and two conventional 4.5% Cu/ZrO_2 and 4.6% Cu/TiO_2 catalysts were used as reference catalysts in the CO oxidation reaction. Conventional supported Cu catalysts were prepared by the wet impregnation method using commercial P25-TiO_2 and ZrO_2 as supports and $Cu(NO_3)_2$ as copper source. Typically, about 300 mg of sample catalyst was diluted with equal weight of glass beads (20–40 mesh) and introduced in a stainless-steel tubular

SCHEME 1: Schematic Representation for the Formation of Nanoporous Network Solids from Alkyl-Chain-Capped Metal/Metal Oxide Nanoparticles (NPs) upon Thermal Procedure

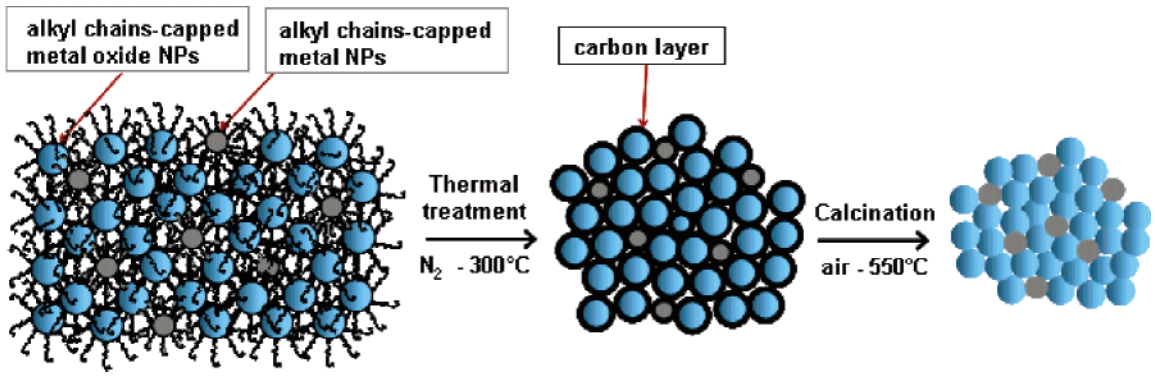

reactor (i.d. = 4 mm). Then the catalyst first was activated by passing a flow of 30 mL/min of dry ultrapure helium at 250 °C and later using a mixture of H_2/helium (10% hydrogen). A stream of 60 mL/min reaction gas mixture containing 2.3% CO, 2.5% O_2, and the balance helium was passed on the catalyst bed at different temperatures for specified times. The reactor effluent was then analyzed by using an online IR gas analyzer (FTLA2000, ADD, Canada). The amounts of CO, CO_2, and oxygen were monitored in reaction products.

Results and Discussion

The synthesis of this class of porous metal/metal oxide NP materials by self-assembly of the presynthesized oleic acid (OA)-capped NPs is performed in organic solvent medium. Owing to capping with the alkyl chains, the resulting NPs are hydrophobic, weak interactions in between and highly dispersed in solvent. A homogeneous mixture of both metal and metal oxide NPs can therefore be obtained. By evaporation of organic solvent, metal and metal oxide NPs are entangled into each other and remain homogeneously dispersed. Since the NPs are protected by alkyl chains, subsequently their catastrophic aggregation can be prevented upon thermal treatment. Apparently, the metal NPs are locked in the voids which are created within the metal oxide NPs compact after organic removal (see Scheme 1). In fact, the capping alkyl chains are acting as protecting agent between NPs to inhibit them from aggregation during the first step of thermal treatment in nitrogen. At the end of this step, the NP surface tension is suppressed; however, NPs still remain isolated. In the following step, carbon layers which were formed on the NP surface are burned out by calcination. As a result, the nanoporous network solids with high surface area and high interparticle porosity can be obtained. In fact, the long alkyl chain surfactants covering the NPs can act as sacrificial spacers between the NPs, which are removed during the thermal procedure, giving rise to a porous structure.

On the basis of this general concept, different types of metal NPs and oxide NPs with desired proportions and almost no limit in their numbers can be simultaneously mixed together, since each of its components is separately presynthesized and preserved in organic solvent.

In this study, we have selected Au and Cu as metal nanoparticles and TiO_2 and ZrO_2 as metal oxide nanoparticles. Toluene and oleic acid (OA) were used as solvent medium and capping agent, respectively. The methods of preparation of these nanoparticles are presented in the Experimental Section. The presynthesized OA-capped NPs were highly dispersed in toluene and, however, precipitated by adding a less hydrophobic solvent, such as ethanol, into the solution (see Supporting Information, S-Figure 1). According to the TEM observation, the as-synthesized nanoparticles exhibit a rather uniform and nearly spherical shape with an average diameter of 7.0, 8.5, 3.1, and 5.0 nm for ZrO_2, TiO_2, Au, and Cu, respectively (S-Figure 2). Table 1 summarizes the physical properties of different types of metal and metal oxide NPs and self-assembled metal/metal oxide NP materials. The particle sizes determined using the Scherrer equation correspond reasonably well to those estimated from the TEM pictures.

The weak interaction between hydrophobic metal nanoparticles and metal oxide nanoparticles in toluene was used for their cooperative assembly. Different combinations of the metal NP solution with the metal oxide NP solution are shown in Figure 1A. The transparent solutions were observed in color, suggesting the homogeneous dispersion of these hydrophobic metal and metal oxide NPs in the solution. Further, to evaluate particle sizes, TEM samples were prepared by dipping carbon-coated Cu grids directly into the solution and drying at room temperature. Representative TEM images of these metal/metal oxide NP samples also indicate a high dispersion of metal NPs on metal oxide NPs network (Figure 1B).

For the OA-capped TiO_2 and ZrO_2 NPs powders after thermal treatment in nitrogen at 300 °C for 2 h, the carbon content is 1.1 and 1.4 wt %, respectively, as measured by TGA-MS analysis, suggesting carbon-coated nanoparticles after this treatment. Furthermore, to prove the oleic acid molecules capped on the NPs surface, two characterization techniques were used: FTIR and XPS. We have carried an FTIR measurement of the oleic acid (OA), OA-capped CuO NPs, OA-capped ZrO_2 NPs, and OA-capped TiO_2 NPs. As seen in Figure 2, IR bands at 2855−2925 cm^{-1} were attributed to the C−H stretching mode of methyl and methylene groups of the oleic acid molecules for all samples. The spectrum of free oleic acid shows an IR band at 1710 cm^{-1} corresponding to the vibration of free −COOH. For the OA-capped NP samples, the IR band at 1710 cm^{-1} was absent; however, two IR bands at 1555 and 1460 cm^{-1} were observed. These bands correspond to the stretching frequency of the carboxylate groups from the oleic acid, which was bonded to the NPs surface.[10] The XPS data at different steps of thermal treatment in situ are summarized in Table 2. High surface concentrations of carbon for as-made TiO_2 and ZrO_2 nanoparticles were observed before and after thermal treatment under N_2 at 300 °C; however, no significant carbon loading was detected after calcination at 550 °C. These clearly indicate carbon shell on each as-made nanoparticles and after N_2 thermal treatment (see Scheme 1).

The metal/metal oxide NP mixtures after thermal treatment (e.g., in nitrogen and then in air) exhibit wormhole-type

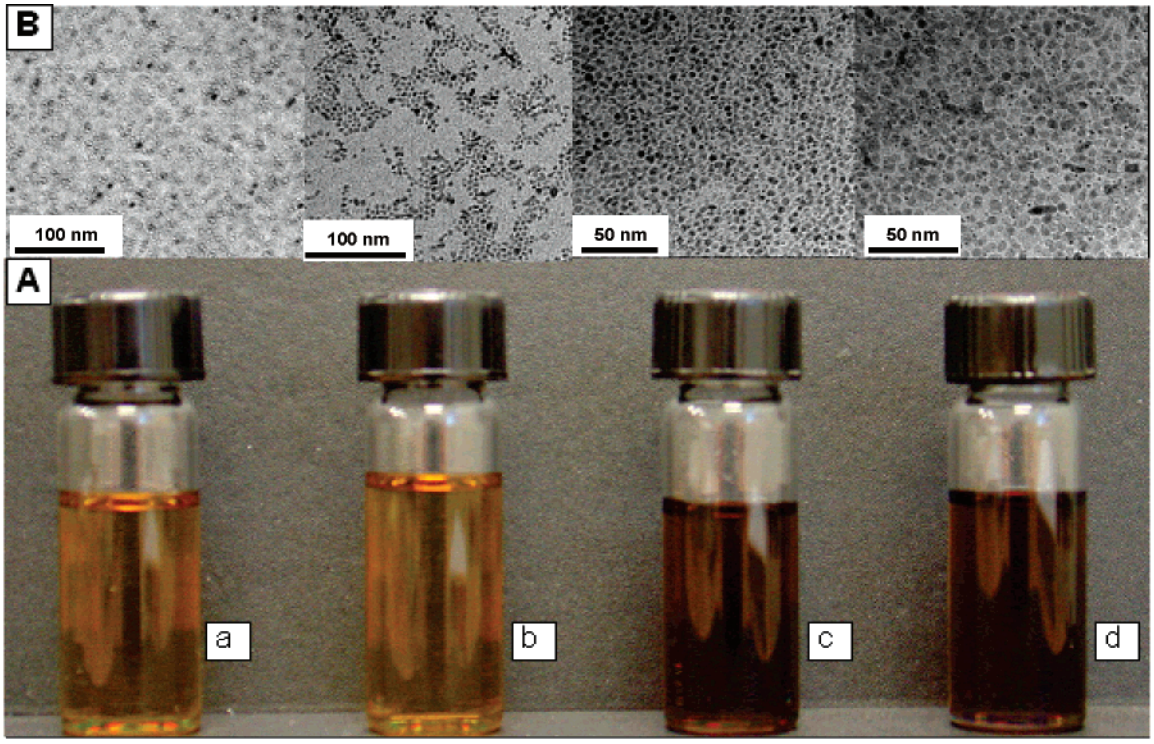

Figure 1. (A) Oleic acid (OA)-capped nanoparticles (NPs) of both metals and metal oxides dispersed in toluene: (a) Cu−ZrO_2 NPs, (b) Cu−TiO_2 NPs, (c) Au−ZrO_2 NPs, and (d) Au−TiO_2 NPs. **(B)** Representative TEM images of as-made mixed metal/metal oxide NPs.

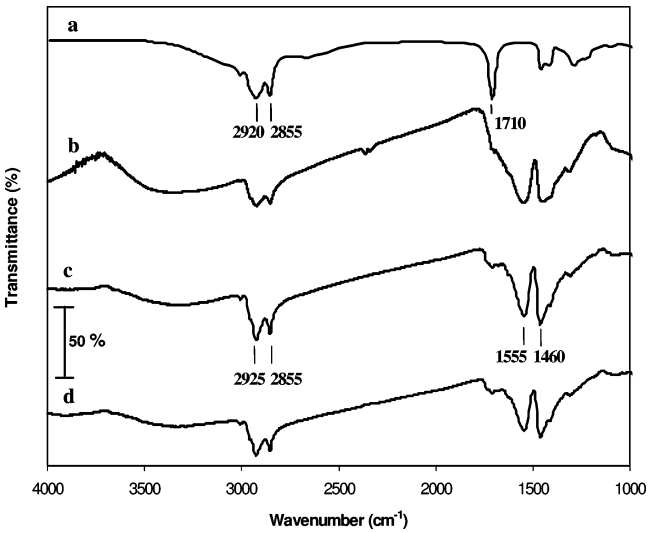

Figure 2. FTIR spectra of (a) free-oleic acid (OA), (b) OA-capped CuO NPs, (c) OA-capped ZrO_2 NPs, and (d) OA- capped TiO_2 NPs (the FTIR spectra for samples a, b, and c are offset vertically by 260, 180, and 80 of transmittance (%), respectively).

nanostructure. The TEM images of the calcined 3.4% Cu/ZrO_2−NP and 3.8% Cu/TiO_2−NP samples reveal homogeneous wormlike mesopores throughout large domains (S-Figure 3). The NPs retained however their individual size and shape.

The nanoporosity within the metal and metal oxide NPs was also shown by nitrogen adsorption/desorption isotherms. A type IV adsorption/desorption isotherm of the calcined samples indicates the presence of mesopore structure (S-Figure 4). The average pore diameter with narrow mesopore size distributions is 3.7 and 4.7 nm, and the BET surface area is 130 and 162 m^2/g for the 3.4% Cu/ZrO_2 NPs and 3.8% Cu/TiO_2 NPs samples, respectively. Interestingly, the theoretical specific surface areas calculated from the TEM average particle sizes, assuming

TABLE 2: XPS Surface Compositions (atom %) of the TiO_2 and ZrO_2 Nanoparticles at Different Steps of Treatment: before Treatment, after Treatment in Nitrogen at 300 °C for 2 h, and Subsequently Calcination in Air at 550 °C for 2 h

NPs sample	element	before treatment (as made sample)	after treatment 300 °C in N_2	after treatment in N_2 followed cal in air −550 °C
ZrO_2	Zr	8.2	22.1	30.7
	O	20.8	47.3	67.2
	C	71.0	30.6	2.1
TiO_2	Ti	19.8	15.6	30.3
	O	44.8	33.0	67.5
	C	35.4	51.4	2.2

spherical nanoparticles, are comparable to those obtained by the BET technique (Table 1). This indicates that the nanoparticle surface was preserved after the thermal procedure.

The SAXRD (small-angle X-ray diffraction) and XRD patterns of the calcined samples are shown in Figure 3. The SAXDP patterns of the calcined 3.4% Cu/ZrO_2 NP and 3.8% Cu/TiO_2 NP samples show a broad peak at ~2θ 0.8° and 0.5°, respectively, which is characteristic of wormhole-type pore lattice (Figure 3A).[11] For the XRD patterns (Figure 3B), almost cubic phase of zirconia for 3.4% Cu/ZrO_2 NPs and only the anatase phase for 3.8% Cu/TiO_2 NPs were observed. The peaks characteristic of Cu are essentially not visible, owning to a low Cu loading. The average NP sizes of ZrO_2 and TiO_2 NPs determined using Scherrer's equation agreed well with those estimated from the TEM pictures. Moreover, no significant change in the particle size of TiO_2 and ZrO_2 was also observed before and after calcination at 550 °C, suggesting thermally stable metal oxide NPs (Table 1). Furthermore, the TEM observation shows that metal NPs were well stabilized against sintering. To evaluate the dispersion and thermal stability of metal NPs in the metal oxide NP matrix, high metal loading samples (10.5% Cu/TiO_2 NP and 9.5% Au/TiO_2 NP samples) were prepared and followed by calcination at 550 °C and

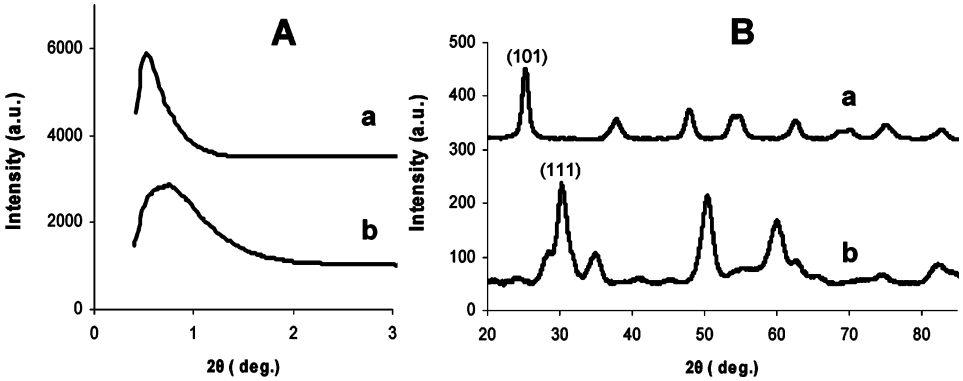

Figure 3. SAXRD patterns (A) and XRD patterns (B) of the metal/metal oxide NPs samples after calcination at 550 °C: (a) 3.8% Cu/TiO_2 NPs and (b) 3.4% Cu/ZrO_2 NPs.

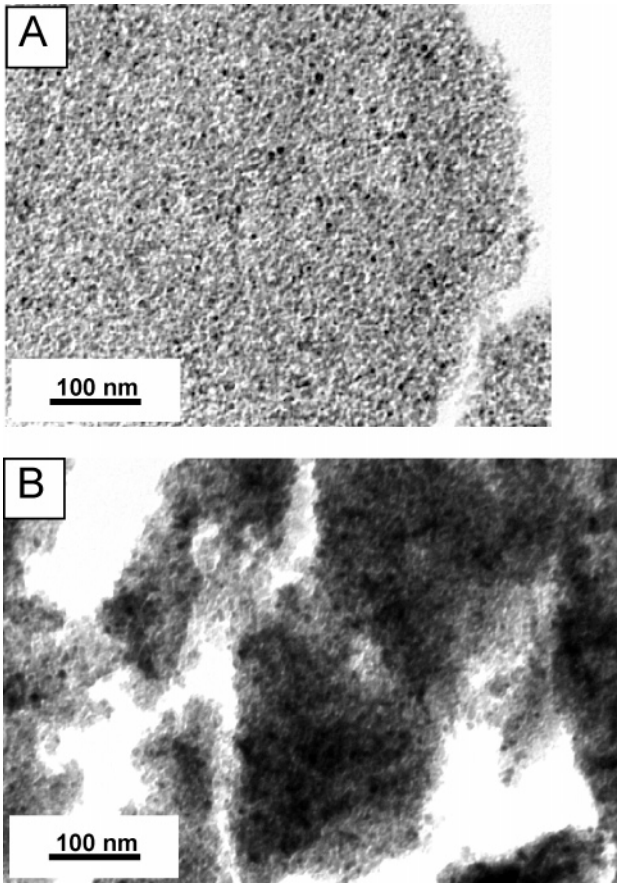

Figure 4. Representative TEM images of nanoporous metal/metal oxide NPs solids after thermal treatment in N_2 at 300 °C and calcination at 550 °C in air followed by H_2 reduction at 300 °C of (A) 9.5% Au−TiO_2 NPs and (B) 10.5% Cu−TiO_2 NPs.

subsequently by reduction at 300 °C. Using an ultra-microtome, ultrathin (∼20 nm) sections of the solid were made after the sample was embedded in a polymeric resin. More than 50 TEM pictures of the samples obtained on numerous parts of the samples show that no obvious aggregation of metal NPs was observed for these samples. Figure 4 shows the representative TEM images of these samples. This indicates that the metal NPs were encapsulated by neighboring metal oxide NPs. As a result, the metal NPs were isolated and randomly distributed throughout the entire NPs network without severe agglomeration.

The CO oxidation conversion over nanoporous Au/oxide NP and Cu/oxide NP catalysts as a function of reaction temperature is shown in S-Figure 5. Commercial noble metal (e.g., Pt/Al_2O_3) and conventional catalyst were used as a reference. To study the effect of Au loading on the catalytic activity, an Au/ZrO_2 NP sample with high Au loading (1.32% Au) was also prepared. The catalytic test conditions are presented in the Experimental Section. S-Figure 6 illustrates the reaction temperature in which the half CO conversion (e.g., 50 mol %) was converted to CO_2. The Au/oxide NP samples are much more active than the commercial Pt/Al_2O_3 catalyst. Further, the 1.32% Au/ZrO_2 NPs sample shows a remarkable catalytic activity with the half CO conversion at below ambient temperature, whereas this conversion was only achieved at temperature as high as 160 °C for the commercial catalyst. Interestingly, the Cu/oxide NP samples of both ZrO_2 and TiO_2 (e.g., no noble metal catalyst) exhibit a higher activity under the same catalytic conditions compared to the commercial noble metal catalyst, Pt/Al_2O_3, and the conventional 4.6% Cu/ZrO_2 and 4.5% Cu/TiO_2 catalysts which were prepared by wet impregnation using commercial P25-TiO_2 and ZrO_2 as support and $Cu(NO_3)_2$ as copper source. Indeed, the half CO conversion on Cu/ZrO_2 NPs sample was obtained at 145 °C, which is 15 °C lower than that of the commercial Pt/Al_2O_3 catalyst. This suggests that the active sites could be affected at the interface of metal−metal oxide NPs. Detailed studies on the catalytic properties of this new type of catalysts are currently underway.

In summary, a simple route has been developed for the synthesis of nanoporous metal/oxide NP materials with high surface area and narrow pore size distribution through the cooperative assembly of alkyl-chain-capped NPs. This simple approach can be considered as a general method and is not limited to one metal/oxide NPs couple. Indeed, nanoporous multicomponent NPs solids with homogeneous dispersion can be synthesized, since each of its components is individually presynthesized with controlled particle size. The high surface area and new properties at the metal/oxide NP interface of such multicomponent NPs solids could make them interesting systems for future studies in many fields of advanced nanotechnology, particularly in catalysis, chemical biological sensors, optics, and electronics.[1,21]

Acknowledgment. This work was supported by the Natural Sciences and Engineering Research Council of Canada (NSERC). The authors thank Profs. S. Kaliaguine and F. Kleitz for stimulating discussions and comments.

Supporting Information Available: Figures showing OA-capped NPs (S-Figure 1), TEM images of OA-capped NPs and nanoporous metal/metal oxide NPs (S-Figures 2, 3), nitrogen adsorption/desorption isotherms of nanoporous metal/metal oxide NPs (S-Figure 4), conversion of CO oxidation over nanoporous metal/metal oxide NPs (S-Figure 5), and half CO

conversion over nanoporous metal/metal oxide NPs (S-Figure 6). This material is available free of charge via the Internet at http://pubs.acs.org.

References and Notes

(1) Astruc, D.; Daniel, M. C. *Chem. Rev.* **2004**, *104*, 293−346. Raimondi, F.; Scherer, G. G.; Kötz, R.; Woraun, A. *Angew. Chem., Int. Ed.* **2005**, *44*, 2190−2209. Park, J.; Joo, J.; Kwon, S. G.; Jang, Y.; Hyeon, T. *Angew. Chem., Int. Ed.* **2007**, *46*, 4630−4660.

(2) Cölfen, H.; Antonietti, M. *Angew. Chem., Int. Ed.* **2005**, *44*, 5576−5591.

(3) Astruc, D.; Lu, F.; Aranzaes, J. R. *Angew. Chem., Int. Ed.* **2005**, *44*, 7852−7872.

(4) Vuong, G. T.; Do, T.-O. *J. Am. Chem. Soc.* **2007**, *129*, 3810−3811.

(5) Zheng, N.; Stucky, G. D. *J. Am. Chem. Soc.* **2006**, *128*, 14278−14280.

(6) Do, T.-O.; Kaliaguine, S. *Angew. Chem., Int. Ed.* **2002**, *41*, 1036−1039.

(7) Do, T.-O.; Kaliaguine, S. *J. Am. Chem. Soc.* **2003**, *125*, 618−619.

(8) Kalsin, A. M.; Paszewski, M.; Smoukov, S. K.; Bishop, K. J. M.; Grzybowski, B. A. *Science* **2006**, *312*, 420−424.

(9) Klajn, R.; Bishop, K. J. M.; Fialkowski, M.; Paszewski, M.; Campbell, C. J.; Gray, T. P.; Grzybowski, B. A. *Science* **2007**, *316*, 261−264.

(10) Zhang, Y. X.; Zeng, H. C. *J. Phys. Chem. C* **2007**, *111*, 6970−6975. Zhang, J.; Ohara, S.; Umetsu, M.; Naka, T.; Hatakeyama, Y.; Adschiri, T.; et al. *Adv. Mater.* **2007**, *19*, 203.

(11) Chane-Ching, J. Y.; Cobo, F.; Aubert, D.; Harvey, H. G.; Airiau, M.; Corma, A. *Chem.—Eur. J.* **2005**, *11*, 979−987.

(12) Pinna, N.; Garnweitner, G.; Antonietti, M.; Niederberger, M. *J. Am. Chem. Soc.* **2005**, *127*, 5608−5612.

(13) Ba, J.; Polleux, J.; Antonietti, M.; Niederberger, M. *Adv. Mater.* **2005**, *17*, 2509−2512.

(14) Carrettin, S.; Concepción, P.; Corma, A.; Nieto, J. M. L.; Puntes, V. F. *Angew. Chem., Int. Ed.* **2004**, *43*, 2538−2540.

(15) Rao, C. N. R.; Kulkarni, G. U.; Thomas, P. J.; Edwards, P. P. A. *Chem.—Eur. J.* **2002**, *8*, 28−35.

(16) Sundar, R. S.; Deevi, S. *J. Nanopart. Res.* **2006**, *8*, 497−509.

(17) Fierro-Gonzalez, J. C.; Bhirud, V. A.; Gates, B. C. *Chem. Commun.* **2005**, 5275−5277.

(18) Abdelsayed, V.; Saoud, K. M.; El-Shall, M. S. *J. Nanopart. Res.* **2006**, *8*, 519−531.

(19) (a) Brust, M.; Bethell, D.; Schiffrin, D.; Kiely, C. J. *Adv. Mater.* **1995**, *7*, 795−797. (b) Brust, M.; Walker, M.; Bethell, D.; Schiffrin, D.; Whyman, R. J. *Chem. Commun.* **1994**, 801−802.

(20) Pan, D.; Zhao, N.; Wang, Q.; Jiang, S.; Ji, X.; An, L. Aranzaes, J. R. *Adv. Mater.* **2005**, *17*, 1991−1995.

(21) Bao, J.; Chen, W.; Liu, T.; Zhu, Y.; Wang, L.; Liu, J.; Wei, Y.; Li, Y. *ACS Nano* **2007**, *1*, 293−298. Nam, J. M.; Thaxton, C. S.; Mirkin, C. A. *Science* **2003**, *301*, 1884−1886.

SUPPORTING INFORMATION

Synthesis of Nanoporous Network Materials with High Surface Areas from the Cooperative Assemblage of Alkyl Chains-Capped Metal/Metal Oxide Nanoparticles

*Driss Mrabet, M. Hassan Zahedi-Niaki and Trong-On Do**

Department of Chemical Engineering, Laval University, Quebec G1K 7P4 Canada

Corresponding author: E-mail: Trong-On.Do@gch.ulaval.ca

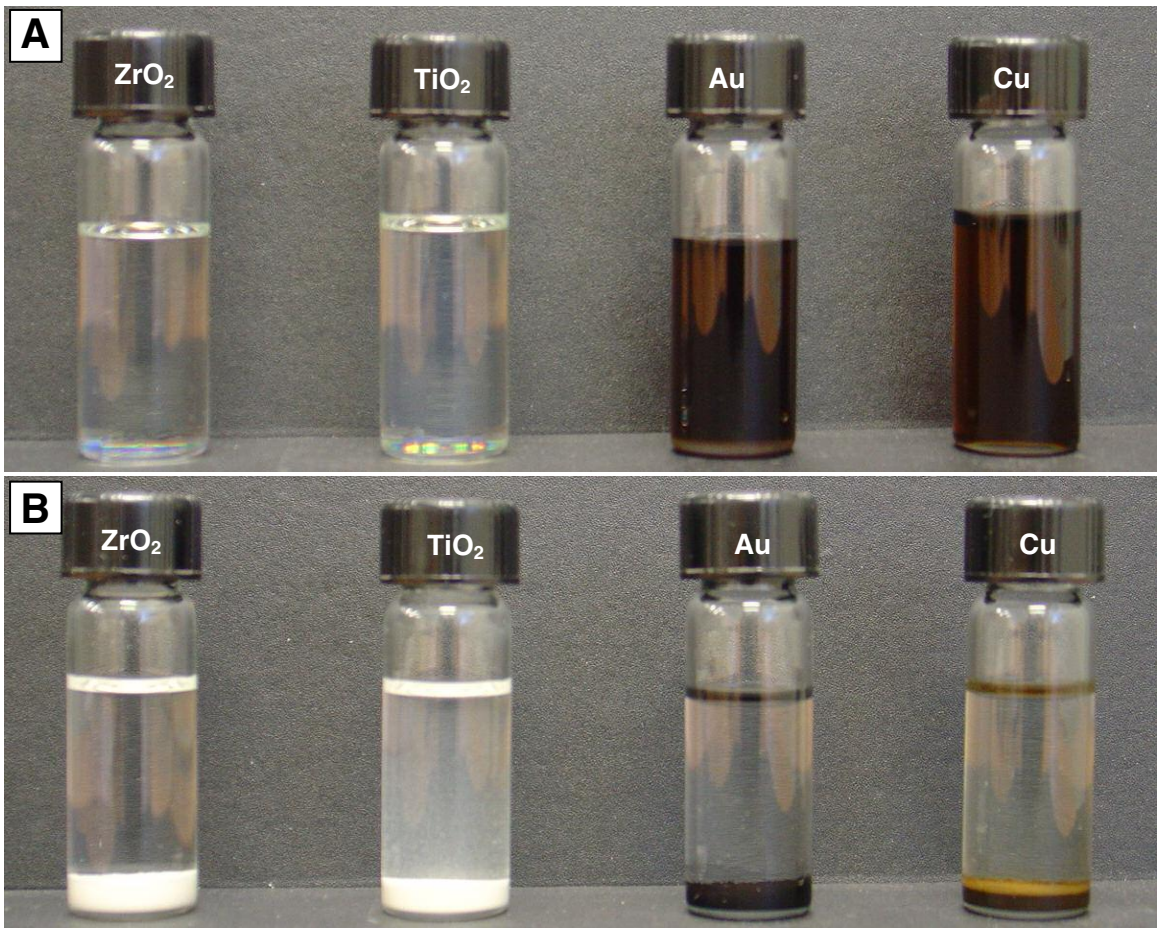

S-Figure 1: **(A)** oleic acid (OA)-capped nanoparticles (NPs) dispersed in toluene of ZrO_2, TiO_2, Au, and Cu (clear/transparent solutions). **(B)** OA-capped nanoparticles precipitated with excess ethanol. (a) TiO_2, (b) ZrO_2, (c) Au, and (d) Cu.

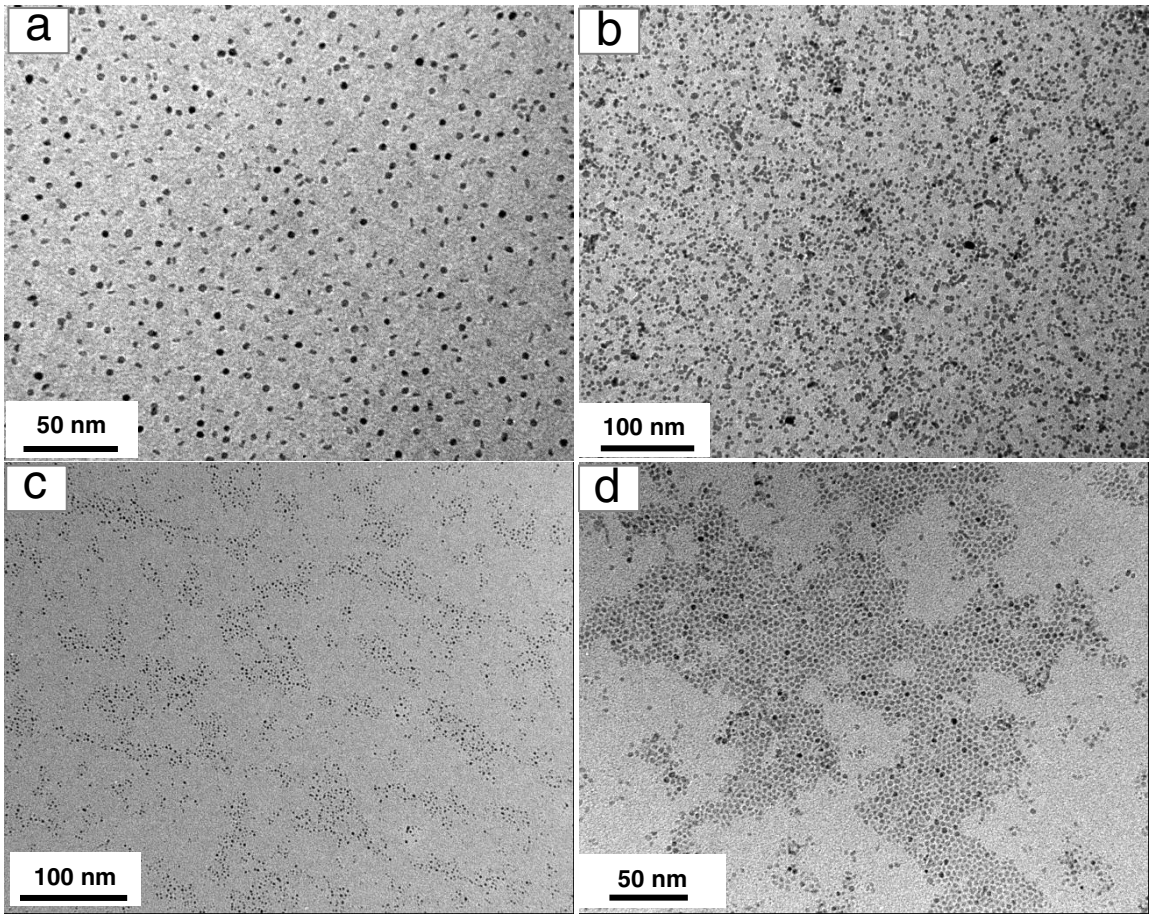

S-Figure 2: TEM images of OA-capped nanoparticles (NPs) of: a) ZrO_2-NPs b) TiO_2-NPs c) Au-NPs, and d) Cu-NPs.

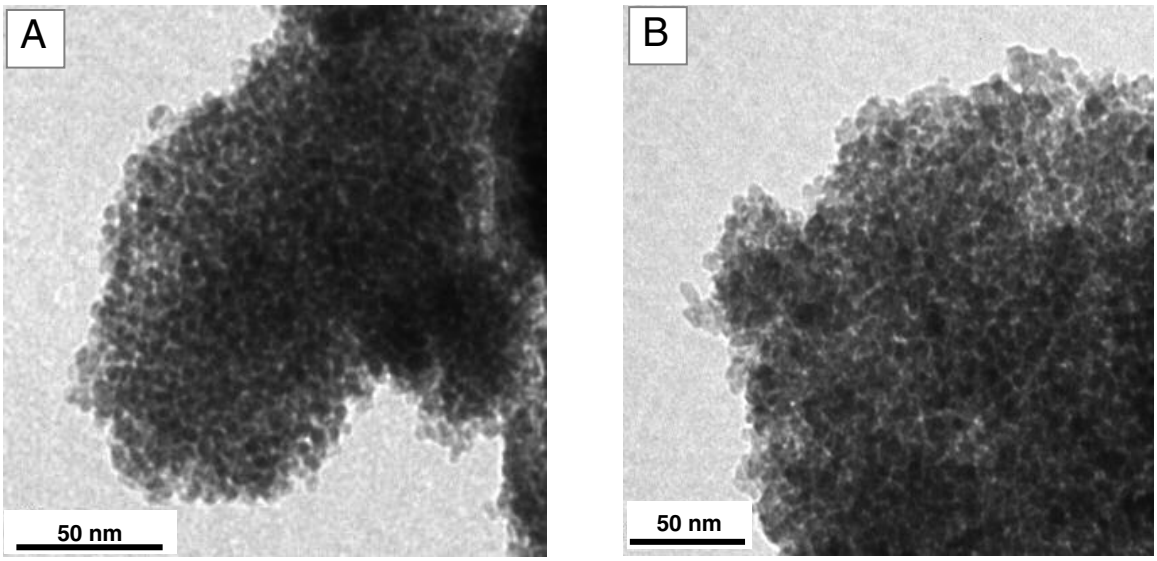

S-Figure 3. Representative TEM images of the nanoporous metal/metal oxide-NPs solids after thermal treatment in N_2 at 300ºC and subsequent calcination at 550ºC in air for 2h of: (A) 3.4%Cu/ZrO_2-NPs, (B) 3.8%Cu-TiO_2-NPs samples.

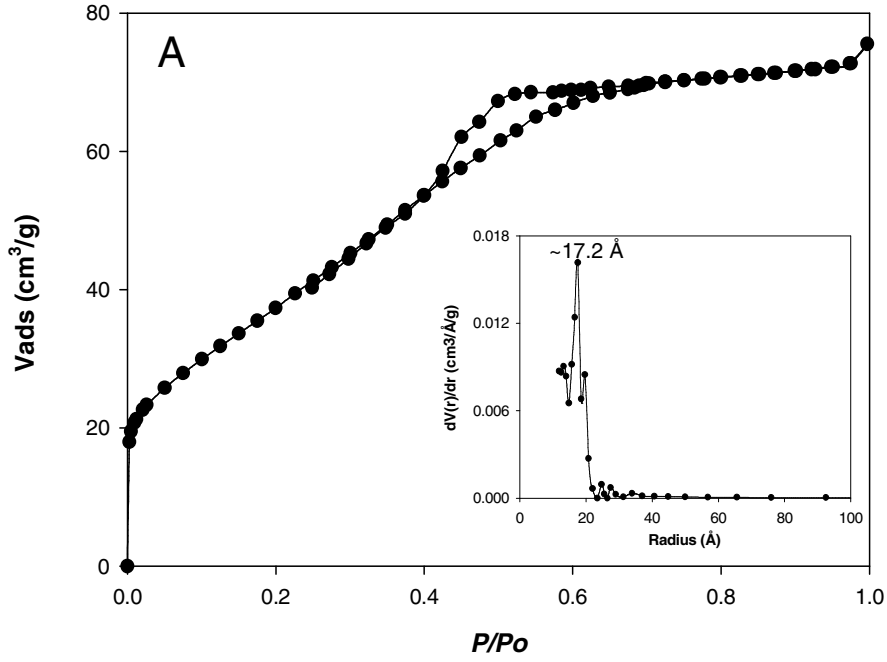

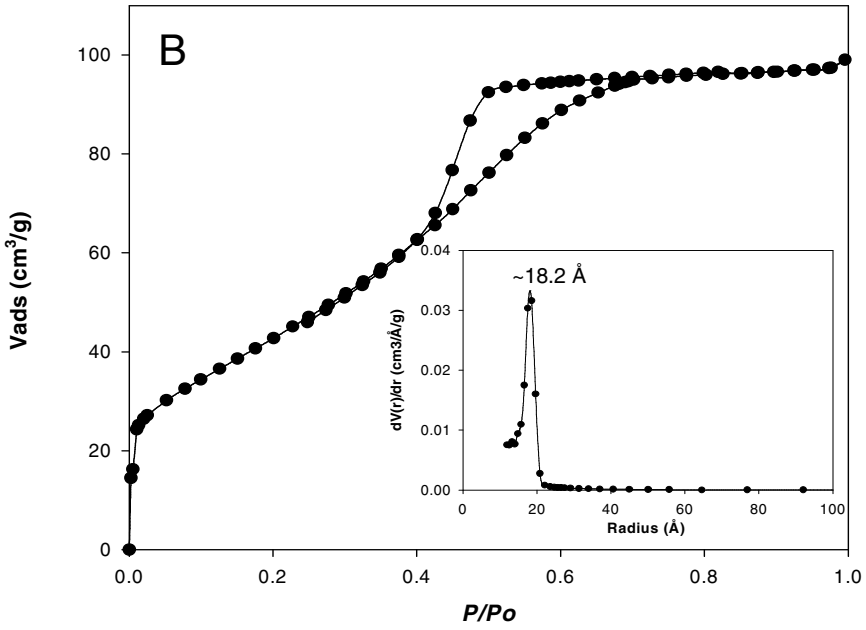

S-Figure 4: Nitrogen adsorption/desorption isotherms and BJH pore radius distribution (inset) of the calcined nanoporous metal/metal oxide NP solids: **(A)** 3.4% Cu-ZrO_2-NPs, **(B)** 3.8% Cu-TiO_2-NPs.

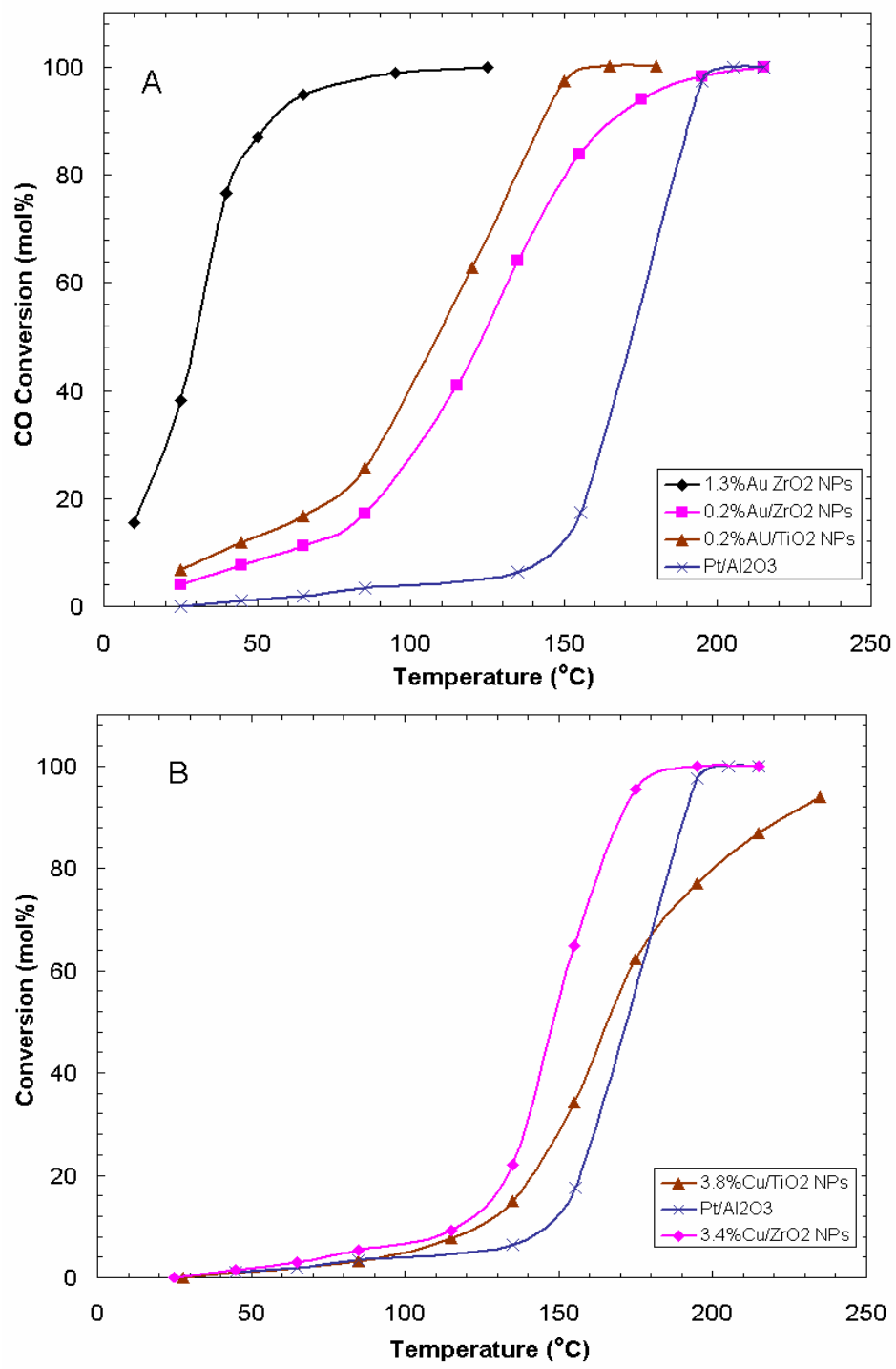

S-Figure 5: Conversion of the CO oxidation over various nanoporous metal/metal oxide samples and the commercial Pt/Al_2O_3.catalyst: **(A)** Au/metal oxide-NPs and **(B)** Cu/metal oxide-NPs

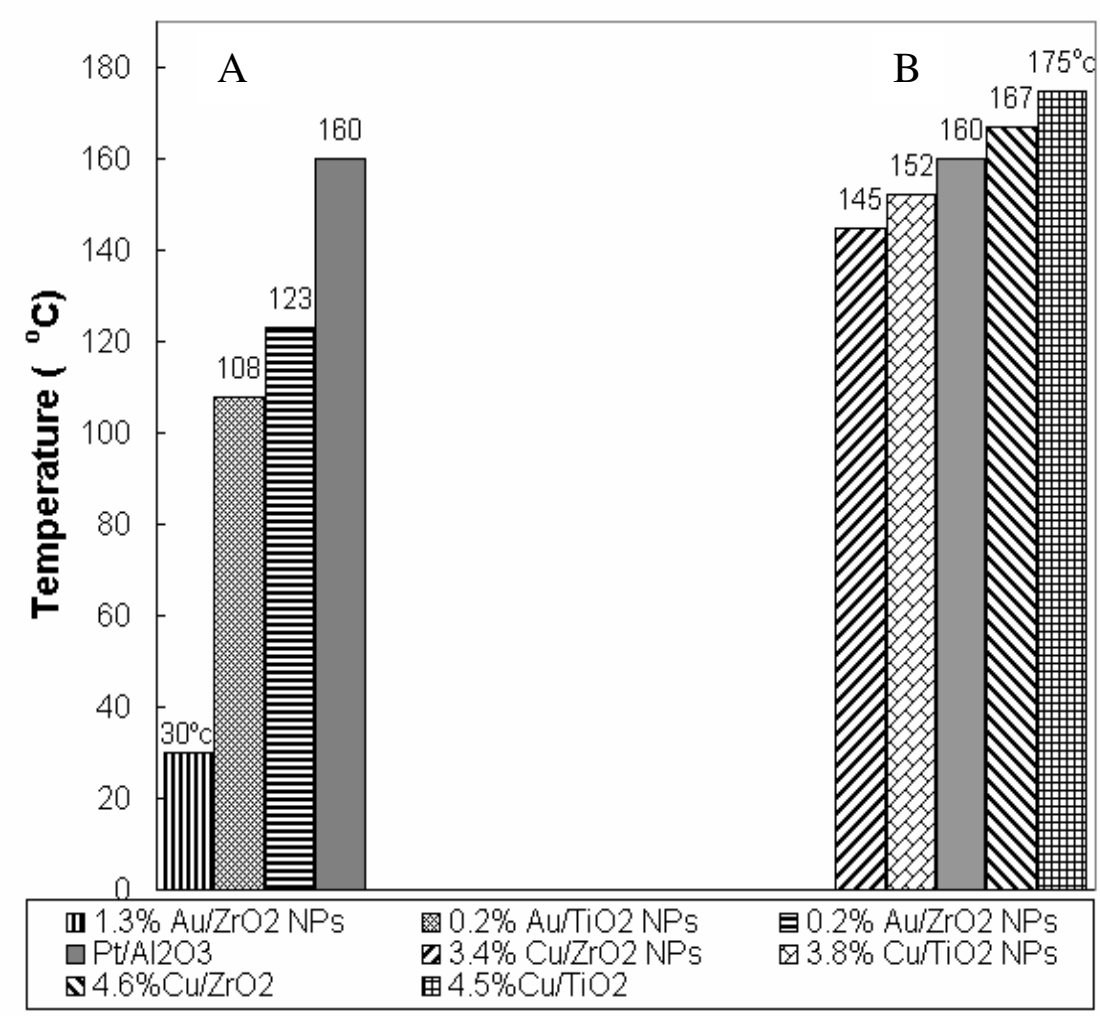

S-Figure 6: Half CO conversion (50 mol.%) over various nanoporous metal/metal oxide catalysts and the commercial Pt/Al_2O_3 and conventional 4.6% Cu/ZrO_2 and 4.5% Cu/TiO_2 catalysts: **(A)** Au/metal oxide-NPs and **(B)** Cu/metal oxide-NPs.